

This article may be downloaded for personal use only. Any other use requires prior permission of the author and AIP Publishing. This article appeared in D'Aguanno, Giuseppe; Sounas, Dimitrios L.; Saied, Hady M.; Alù, Andrea; Nonlinearity-based circulator; Applied Physics Letters 114, 181102 (2019); <https://aip.scitation.org/doi/10.1063/1.5094736> and may be found at <https://aip.scitation.org/doi/10.1063/1.5094736>. Access to this work was provided by the University of Maryland, Baltimore County (UMBC) ScholarWorks@UMBC digital repository on the Maryland Shared Open Access (MD-SOAR) platform.



Please provide feedback

Please support the ScholarWorks@UMBC repository by emailing scholarworks-group@umbc.edu and telling us what having access to this work means to you and why it's important to you. Thank you.

Nonlinearity-based circulator

Cite as: Appl. Phys. Lett. **114**, 181102 (2019); <https://doi.org/10.1063/1.5094736>

Submitted: 05 March 2019 . Accepted: 16 April 2019 . Published Online: 07 May 2019

Giuseppe D'Aguanno, Dimitrios L. Sounas, Hady M. Saied , and Andrea Alù 



View Online



Export Citation



CrossMark

ARTICLES YOU MAY BE INTERESTED IN

[Nonlinear XUV-optical transient grating spectroscopy at the Si L_{2,3}-edge](#)

Applied Physics Letters **114**, 181101 (2019); <https://doi.org/10.1063/1.5085413>

[Inverse design of photonic topological state via machine learning](#)

Applied Physics Letters **114**, 181105 (2019); <https://doi.org/10.1063/1.5094838>

[Multiple non-diffracting beams by reflective surface based on admittance superposition](#)

Applied Physics Letters **114**, 181104 (2019); <https://doi.org/10.1063/1.5090318>

Hall Effect Measurement Handbook

A comprehensive resource for researchers

Explore theory, methods, sources of errors, and ways to minimize the effects of errors



Nonlinearity-based circulator

Cite as: Appl. Phys. Lett. **114**, 181102 (2019); doi: [10.1063/1.5094736](https://doi.org/10.1063/1.5094736)

Submitted: 5 March 2019 · Accepted: 16 April 2019 ·

Published Online: 7 May 2019



View Online



Export Citation



CrossMark

Giuseppe D'Aguanno,^{1,2} Dimitrios L. Sounas,^{1,3} Hady M. Saied,^{4,5}  and Andrea Alu^{1,4,5,6,a)} 

AFFILIATIONS

¹Department of Electrical and Computer Engineering, The University of Texas at Austin, Austin, Texas 78712, USA

²Department of Computer Science and Electrical Engineering, University of Maryland, 1000 Hilltop Circle, Baltimore, Maryland 21250, USA

³Department of Electrical and Computer Engineering, Wayne State University, Detroit, Michigan 48202, USA

⁴Photonics Initiative, Advanced Science Research Center, City University of New York, New York, New York 10031, USA

⁵Department of Electrical Engineering, City College of the City University of New York, New York, New York 10031, USA

⁶Physics Program, Graduate Center, City University of New York, New York, New York 10016, USA

^{a)}Author to whom correspondence should be addressed: aalu@gc.cuny.edu.

ABSTRACT

Commercially available nonreciprocal devices, such as isolators and circulators, play a fundamental role in communication systems. Since they commonly rely on magnetic materials, they tend to become bulky, expensive, and difficult to be integrated in conventional microelectronic circuits. Here, we explore the functionality of a magnetic-free circulator where reciprocity is broken by suitable geometric asymmetries combined with tailored nonlinearities. We show that it is possible to operate a fully passive coupled resonator system without external bias like a circulator for pulsed signals impinging at its ports within a desired range of intensities. The functionality can be applied to a variety of physical systems, ranging from electronics to photonics and acoustics.

Published under license by AIP Publishing. <https://doi.org/10.1063/1.5094736>

According to Lorentz reciprocity, signal transmission between two points in space is the same for opposite propagation directions.^{1–5} In other words, if a signal can propagate from point *A* to point *B* through a given channel, the reversed propagation path from point *B* to point *A* is also possible with equal strength. There are several situations in which we want to transmit signals breaking this symmetry. For example, in full-duplex communication systems,⁶ unidirectional signal transmission from the transmitter to the antenna and, at the same time, isolation of the receiver from self-interference are sought after. In optics, source protection from back reflections and interferences is very important to avoid detuning. These are examples for which we need to operate outside the domain of validity of Lorentz reciprocity theorem.⁷

Reciprocity is valid under the assumption that the electric permittivity tensor ϵ and the magnetic permeability tensor μ of the involved materials in the propagation channel are: (a) time-reversal symmetric, (b) time-independent, and (c) linear. The most common approach to achieve nonreciprocal devices is therefore to break the symmetry of the electric permittivity tensor, which can be achieved by applying an external magnetic field to a ferromagnetic medium.⁸ As a result, circularly polarized electromagnetic waves with opposite rotation directions interact differently with such media, and reciprocity is

broken. Although biasing the material with a magnetic field is the most common way to break reciprocity, it is not the only one. Recently, magnetic-free circulators and isolators based on the time modulation of the electric permittivity of the medium have been studied both theoretically and experimentally.^{9–12} While this approach relaxes the need of special materials supporting magneto-optical phenomena, it still requires sufficiently fast temporal modulations, which are not necessarily easy or convenient to implement. Exploiting nonlinearities can alleviate this need since through nonlinearities, the signal itself traveling through the device can impart a form of bias, breaking reciprocity. Indeed, nonreciprocal propagation in one-dimensional structures exploiting quadratic or cubic nonlinearities has been proposed in the past and recent times^{13–18} although these approaches have limitations in their operation stemming from thermodynamic considerations¹⁹ and are restricted to nonsimultaneous excitation from different ports.²⁰

The vast majority of nonlinearity-induced nonreciprocal devices proposed to date have been limited to two-port operation. Circulators, on the other hand, are three-port devices where an electromagnetic signal applied to Port 1 only comes out from Port 2 (or Port 3), a signal applied to Port 2 only comes out from Port 3 (or Port 2), and a signal applied to Port 3 only comes out of Port 1 (or Port 2). In other

words, the electromagnetic signals circulate in a preferred direction, either clockwise or counterclockwise, an ideal operation to realize full-duplex communications, connecting the transmitter, receiver, and antenna to the three ports of the device.

Consistent with the previous discussion, commercial circulators rely on magnetic materials, which make them bulky, expensive, and not CMOS compatible. Here, we explore the functionality of bias-free, fully passive nonlinear circulators with isolation factors that exceed 20 dB. A nonlinear magnetless circulator was presented in Ref. 17, but required the use of active materials, in contrast to the fully passive design proposed in the following.

We start in Fig. 1(a) by sketching the generic layout of our circulator. The structure consists of a loop of six identical coupled resonators interlaced by alternating linear and nonlinear coupling coefficients.

Due to the rotational symmetry of the structure, a circulator response can be accomplished if, for excitation from any port (e.g., port 1), we achieve zero transmission to one of the other ports (e.g., port 2) and maximum transmission to the third one (e.g., port 3). Such a network of coupled resonators can be efficiently described through coupled mode theory²¹ as

$$\begin{aligned} i\dot{a}_1^{(A)} &= \omega_0 a_1^{(A)} + \kappa_0 a_3^{(B)} + \left(\kappa_1 + \alpha |a_1^{(A)} - a_1^{(B)}|^2 \right) a_1^{(B)} \\ &\quad - i\Gamma a_1^{(A)} + i\sqrt{2}\Gamma e^{-i\omega t}, \end{aligned} \quad (1a)$$

$$i\dot{a}_2^{(A)} = \omega_0 a_2^{(A)} + \kappa_0 a_1^{(B)} + \left(\kappa_1 + \alpha |a_2^{(A)} - a_2^{(B)}|^2 \right) a_2^{(B)} - i\Gamma a_2^{(A)}, \quad (1b)$$

$$i\dot{a}_3^{(A)} = \omega_0 a_3^{(A)} + \kappa_0 a_2^{(B)} + \left(\kappa_1 + \alpha |a_3^{(A)} - a_3^{(B)}|^2 \right) a_3^{(B)} - i\Gamma a_3^{(A)}, \quad (1c)$$

$$i\dot{a}_1^{(B)} = \omega_0 a_1^{(B)} + \kappa_0 a_2^{(A)} + \left(\kappa_1 + \alpha |a_1^{(A)} - a_1^{(B)}|^2 \right) a_1^{(A)}, \quad (1d)$$

$$i\dot{a}_2^{(B)} = \omega_0 a_2^{(B)} + \kappa_0 a_3^{(A)} + \left(\kappa_1 + \alpha |a_2^{(A)} - a_2^{(B)}|^2 \right) a_2^{(A)}, \quad (1e)$$

$$i\dot{a}_3^{(B)} = \omega_0 a_3^{(B)} + \kappa_0 a_1^{(A)} + \left(\kappa_1 + \alpha |a_3^{(A)} - a_3^{(B)}|^2 \right) a_3^{(A)}. \quad (1f)$$

In Eq. (1), $a_j^{(A)}$ and $a_j^{(B)}$, with $j = 1, 2, 3$, are the time-dependent field amplitudes at the A and B j -th resonator, respectively, ω_0 is the uncoupled resonators' resonant frequency, $\kappa_0 > 0$ is the linear coupling coefficient, $\kappa_1 > 0$ is the linear part of the nonlinear coupling coefficient, α is the nonlinear parameter, $\Gamma = 1/\tau$ is the coupling loss term, where τ is the average lifetime (dwell time) of the radiation in the resonators before the energy is released to Port 2 and Port 3, and, finally, $\sqrt{2}\Gamma e^{-i\omega t}$ is the input signal (forcing term) at Port 1 oscillating at frequency ω . In our system, resonators A_j with $j = 1, 2, 3$ have a termination at Port- j , while resonators B_j have no port termination. We now look for steady-state solutions of Eq. (1) in the form $a_j^{(k)}(t) = c_j^{(k)} e^{-i\omega t}$, with $k = A, B$ and $j = 1, 2, 3$, where $c_j^{(k)}$ is the time independent amplitude of the field. The reflectance at Port 1 (R_1) and transmittances at Port 2 and Port 3 (T_2 and T_3) are given by $R_1 = |\sqrt{2}\Gamma c_1^{(A)} - 1|^2$ and $T_2 = 2\Gamma |c_2^{(A)}|^2$ and $T_3 = 2\Gamma |c_3^{(A)}|^2$, respectively, and power conservation dictates that $R_1 + T_2 + T_3 = 1$. For the case of linearly coupled resonators and no coupling loss ($\alpha = 0$ and $\Gamma = 0$), the system admits four resonant frequencies (eigenfrequencies), given by $\omega_0 \pm (\kappa_1 + \kappa_0)$ and $\omega_0 \pm \sqrt{\kappa_1^2 - \kappa_1 \kappa_0 + \kappa_0^2}$. When the electromagnetic signal applied to Port 1 oscillates with a frequency close to one of the eigenfrequencies of the system, then energy is efficiently coupled with the resonators and eventually is expected to be transmitted to Port 2 and Port 3; otherwise, the signal is mostly reflected at Port 1.

In the linear regime ($\alpha = 0$), because of symmetry, the power output at Port 2 is equal to the power output at Port 3 ($T_2 = T_3$), regardless of the specific values of linear coupling coefficients κ_0 and κ_1 . In order to shed some light on the nonlinear behavior of the system, we look for nonlinear solutions that can support complete isolation at Port 2. In other words, we look for solutions that support the condition of zero field at Port 2, i.e., $c_2^{(A)} = 0$. For $\kappa_0 = \kappa_1$ at the resonant frequency $\bar{\omega} = \omega_0 + \kappa_0$, we find the following solutions:

$$\begin{aligned} c_1^{(A)} &= c_1^{(B)} = \frac{1}{\sqrt{2}\Gamma} (1 + \delta) e^{-i\bar{\omega}t}, \quad c_2^{(B)} = c_3^{(A)} = -\frac{1}{\sqrt{2}\Gamma} e^{-i\bar{\omega}t}, \\ c_3^{(B)} &= i\frac{\sqrt{\Gamma/2}}{\kappa_0} (-1 + \delta) e^{-i\bar{\omega}t}, \end{aligned} \quad (2)$$

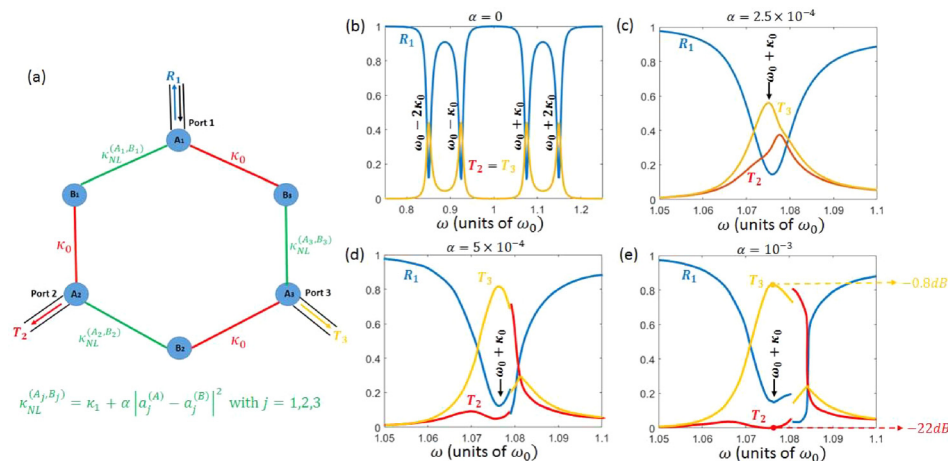


FIG. 1. (a) 3-Port circulator made of a closed loop of six resonators with resonant frequency ω_0 interlaced by an alternation of linear (κ_0) and nonlinear ($\kappa_{NL}^{(A_j, B_j)} = \kappa_1 + \alpha |a_j^{(A)} - a_j^{(B)}|^2$) coupling coefficients, where $\alpha > 0$ is the nonlinear parameter. (b) Reflectance (R_1) at Port 1 (input port) and transmittance at Port 2 (T_2) and Port 3 (T_3) for the linear case ($\alpha = 0$), $\kappa_0 = \kappa_1 = 0.075\omega_0$, and coupling loss $\Gamma = 0.012\omega_0$. (c)–(e) Reflectance and transmittances around the resonant frequency $\omega_0 + \kappa_0$ for increasing values of the nonlinearity parameter. More than 20 dB isolation at Port 3 is achieved in (e).

with $\delta = \alpha/2\Gamma\kappa_0$. It can be easily ascertained by direct substitution that Eq. (2) satisfies Eqs. (1a), (1b), (1d), and (1e) under the conditions specified above, i.e., $c_2^{(A)} = 0$, $\kappa_0 = \kappa_1$, and $\bar{\omega} = \omega_0 + \kappa_0$. Under the same conditions, Eq. (2) satisfy Eqs. (1c) and (1f) on the order of δ for $\delta \ll 1$ and $\Gamma/\kappa_0 \sim \delta^2$. This can also be easily verified by substituting Eq. (2) into Eqs. (1c) and (1f) and neglecting the terms of order δ^2 and higher. Physically speaking, the condition $\delta \ll 1$ means that the nonlinearity is a perturbation, while $\Gamma/\kappa_0 \sim \delta^2$ amounts to require high-quality (Q) resonators. The solutions in Eq. (2) lead to $R_1 = |\sqrt{2\Gamma}c_1^{(A)} - 1|^2 = \delta^2$, $T_2 = 2\Gamma|c_2^{(A)}|^2 = 0$ and $T_3 = 2\Gamma|c_3^{(A)}|^2 = 1$, and $R_1 + T_2 + T_3 = 1 + \delta^2$, and therefore, power is conserved on the order of δ , consistent with the functionality investigated here. Hence, our analysis suggests that at the resonant frequency $\omega_0 + \kappa_0$, the electromagnetic energy can be almost completely routed to Port 3, almost perfect isolation at Port 2 is achieved, and reciprocity is largely broken.

This theoretical result is indeed confirmed by a full numerical integration of Eq. (1) in the time domain, as shown in Figs. 1(b)–1(e). In the linear case [Fig. 1(b)], four transmission resonances are found at the eigenfrequencies of the system, and transmission resonances at Port 2 and Port 3 are exactly the same, as expected. By increasing the nonlinear parameter (other panels in Fig. 1), the two transmission resonances at $\omega_0 + \kappa_0$ depart from each other. Eventually, transmission at Port 2 becomes almost completely quenched, and most of the energy is routed to Port 3, with an isolation factor of more than 20 dB. We also note that at higher frequencies, the system undergoes an abrupt transition, switching to another stable state of the nonlinear system, with energy mostly routed to Port 2. In order to further corroborate this analysis, in Fig. 2, we present the results of a numerical simulation in the parameter space (α, Γ) . In particular, in Figs. 2(a)–2(c), we show the transmittance and reflectance coefficients as a function of (α, Γ) at the frequency $\omega_0 + \kappa_0$ for α varying from $10^{-4}\omega_0^2$ to $10^{-3}\omega_0^2$ and Γ varying from $10^{-3}\omega_0$ to $2 \times 10^{-2}\omega_0$. The highest isolation of 23 dB is reached for $\alpha = 10^{-4}\omega_0^2$ and $\Gamma = 3 \times 10^{-3}\omega_0$. Figure 2(d) shows the corresponding reflection and transmission curves vs frequency for this scenario.

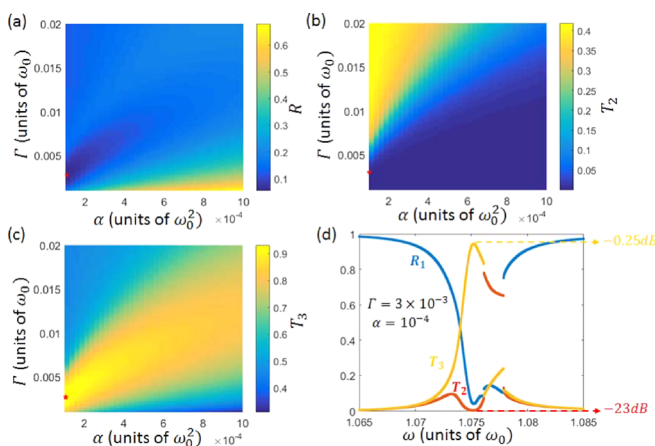


FIG. 2. (a)–(c) Reflectance and transmittance at $\omega_0 + \kappa_0$ in the (α, Γ) plane for $\kappa_0 = \kappa_1 = 0.075\omega_0$. The stars indicate the point in the parameter space where the largest isolation factor is reached. (d) Frequency dispersion corresponding to the point of largest isolation.

So far, in our analysis, we have considered the particular case in which $\kappa_0 = \kappa_1$ because in such a case, it is possible to solve analytically for the value of isolation at Port 2 at the eigenfrequency $\omega_0 + \kappa_0$. Nevertheless, qualitatively similar results are obtained when $\kappa_0 \neq \kappa_1$. In this case, the isolation at Port 2 arises close to the eigenfrequency $\omega_0 + \sqrt{\kappa_1^2 - \kappa_1\kappa_0 + \kappa_0^2}$. An example of this more general scenario is provided in Fig. 3. By increasing the nonlinearity coefficient further with respect to the case shown in Fig. 3(d), isolation factors exceeding 20 dB are obtained although in the latter case, the frequency where isolation is achieved blue-shifts with respect to the position of the eigenfrequency of the linear scenario.

In order to verify the proposed concept, a realistic radio-frequency circuit—shown in Fig. 4—has been designed, optimized, and numerically simulated for realistic circuit parameters, including parasitics, as detailed in the table in Fig. 4. The resonators are chosen in the parallel resonance configurations, while the coupling elements are realized through nonlinear capacitors and impedance inverters for the nonlinear and linear coupling elements, respectively, as sketched in the insets, while the corresponding coupling coefficients are found in Refs. 22 and 23. Impedance inverters⁸ were chosen to avoid that the coupling elements affect the resonator impedances, enabling a simpler optimization procedure. The table in Fig. 4 provides the correspondence between the CMT parameters and the circuit elements. Following the results in our approximate analytical model described above, first, we investigated the low-intensity scenario using a full-wave circuit simulator with circuit parameter values $\Gamma = 0.0125$, $k_k = 0.043$, and $k_n = 0.021$. Figure 5(a) shows the corresponding reflectance and transmittance, which follow well the predicted results in Figs. 1 and 3. Next, we considered realistic nonlinearities as the input intensity is increased. For the same circuit parameters and nonlinearity coefficient $\alpha = 0.212$, circulator operation is found around the first peak of the transmission coefficient, consistent with the previous analysis [Fig. 5(b)]. Finally, we further increased the input power, yielding in Fig. 5(c) an isolation above 17 dB and an insertion loss of 0.57 dB

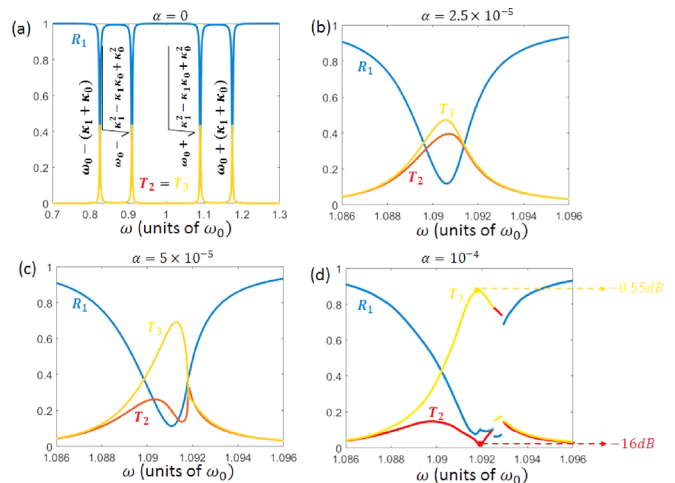


FIG. 3. (a) Reflectance and transmittance in the linear case for $\kappa_0 = 0.075\omega_0$, $\kappa_1 = 0.1\omega_0$, and coupling loss $\Gamma = 0.003\omega_0$. (b)–(d) Reflectance and transmittance around the resonant frequency at $\omega_0 + \sqrt{\kappa_1^2 - \kappa_1\kappa_0 + \kappa_0^2}$ for increasing values of the nonlinearity parameter.

C_m	$C_o(1 + \alpha V^2)$
k_n	$\frac{1}{2} \frac{C_m}{C_o} \omega_o$
C_k	$\frac{1}{Z_k \omega_o}$
L_k	$\frac{Z_k}{\omega_o}$
k_k	$\frac{1}{2} \frac{Z_o}{Z_k} \omega_o$
ω_o	$\frac{1}{\sqrt{L_o C_o}}$
Z_o	$\sqrt{\frac{L_o}{C_o}}$
Γ_i	$\frac{1}{C_o \omega_o R_i}$

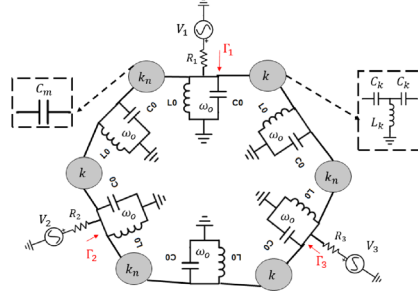


FIG. 4. The proposed RF circuit, composed of 6 parallel resonance resonators, 3 linear coupling elements formed by impedance inverters, and 3 nonlinear coupling elements formed by nonlinear capacitors C_m . The corresponding parameters are shown in the table.

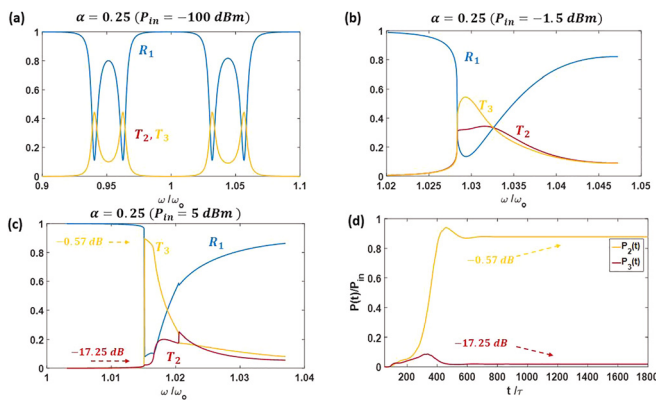


FIG. 5. (a) Reflectance and transmittance in the linear case for $\kappa_n = 0.025\omega_o$, $\kappa_k = 0.043\omega_o$, and coupling loss $\Gamma = 0.0125\omega_o$. (b) and (c) Reflectance and transmittance for increasing values of the nonlinear parameter. (d) Envelope of instantaneous power delivered to both ports normalized to the total input power ($P_{in} = 3$ mW) from the source.

with an input power of 3 mW, in very good agreement with the coupled mode theory model for the case $\kappa_0 \neq \kappa_1$ shown in Fig. 3(d). We have also analyzed the circuit in the time domain to verify the stability and the speed of the response. The envelope of the instantaneous power at the two output ports is plotted in Fig. 5(d) after normalization to the total input power from the source. Very good agreement with the frequency domain analysis is observed, confirming the practical realizability of this concept.

In conclusion, in this work, we have shown the concept and realistic design of a magnet-free, nonbiased, fully passive nonlinear circulator. Nonlinearities are ubiquitous in several physical systems, and therefore, our analysis, based on temporal coupled mode theory for a resonator network, is broadly applicable to a wide variety of practical problems, from passive circulators for radio-wave communications and radars to nanophotonic and quantum computing systems and

acoustics. Our realistic simulations of a passive nonlinear circuit confirm the accuracy of our model and the realistic possibility of realizing a low-loss, fully passive, largely nonreciprocal circulator in which the signal itself, interacting with nonlinearities, breaks reciprocity and induces large isolation. The limitations outlined for other nonlinear, self-biased nonreciprocal devices in the recent literature^{19,20} apply also here, especially in the context of simultaneous excitation from multiple ports. The results in this paper have been derived for continuous wave excitation from a single port at a time, but they are expected to change when multiple continuous waves excite the device from the different ports, because of the nonlinearities. In this sense, pulsed operation is required to operate the circulator in its described functionality. This obvious deficiency may be compensated for some application by the inherent advantage of not requiring any form of bias and its full passivity, making this device particularly appealing for pulsed operation applications, such as in radar or lidar, defense-related, automotive and imaging systems. In applications for which transmitted and received pulses may have different strengths, the present approach may be generalized to asymmetric designs with different intensity thresholds for the different ports. This work was supported by the Air Force Office of Scientific Research.

REFERENCES

- L. Landau and E. Lifshitz, *Electrodynamics of Continuous Media* (Pergamon Press, 1966).
- C. A. Balanis, *Engineering Electromagnetics* (Wiley, 1989).
- L. Onsager, *Phys. Rev.* **37**, 405 (1931).
- H. B. G. Casimir, *Rev. Mod. Phys.* **17**, 343 (1945).
- R. J. Potton, *Rep. Prog. Phys.* **67**, 717–754 (2004).
- M. Duarte, C. Dick, and A. Sabharwal, *IEEE Trans. Wireless Commun.* **11**, 4296 (2012).
- D. J. Alas, A. Petrov, M. Eich, W. Freude, S. Fan, Z. Yu, R. Baets, M. Popović, A. Melloni, J. D. Joannopoulos *et al.*, *Nat. Photonics* **7**, 579 (2013).
- D. M. Pozar, *Microwave Engineering*, 3rd ed. (Wiley, Hoboken, NJ, USA, 2005).
- Z. Yu and S. Fan, *Nat. Photonics* **3**, 91 (2009).
- H. Lira, Z. Yu, S. Fan, and M. Lipson, *Phys. Rev. Lett.* **109**, 33901 (2012).
- N. A. Estep, D. L. Sounas, J. Soric, and A. Alù, *Nat. Phys.* **10**, 923 (2014).
- D. L. Sounas and A. Alù, *Nat. Photonics* **11**, 774 (2017).
- M. D. Tocci, M. J. Bloemer, M. Scalora, J. P. Dowling, and C. M. Bowden, *Appl. Phys. Lett.* **66**, 2324 (1995).
- K. Gallo, G. Assanto, K. R. Parameswaran, and M. M. Fejer, *Appl. Phys. Lett.* **79**, 314 (2001).
- F. Biancalana, *J. Appl. Phys.* **104**, 093113 (2008).
- S. V. Zhukovsky and A. G. Smirnov, *Phys. Rev. A* **83**, 023818 (2011).
- P. Aleahmad, M. Khajavikhan, D. Christodoulides, and P. LiKamWa, *Sci. Rep.* **7**, 2129 (2017).
- D. L. Sounas, J. Soric, and A. Alù, *Nat. Electron.* **1**, 113 (2018).
- D. L. Sounas and A. Alù, *IEEE Antennas Wireless Propag. Lett.* **17**, 1958 (2018).
- Y. Shi, Z. Yu, and S. Fan, *Nat. Photonics* **9**, 388 (2015).
- H. A. Haus and W. Huang, *Proc. IEEE* **79**, 1505 (1991).
- H. A. Haus, *Waves and Fields in Optoelectronics* (Prentice Hall, Incorporated, 1984).
- G. L. Matthaei, L. Young, and E. M. T. Jones, *Microwave Filters, Impedance-Matching Networks, and Coupling Structures* (Artech House, Inc., Norwood, 1980).